Int J Adv Manuf Technol (2017) 88:3217–3232
DOI 10.1007/s00170-016-9023-4

ORIGINAL ARTICLE

Influence of friction models on FE simulation results of orthogonal cutting process

Amir Malakizadi[1] · Keyvan Hosseinkhani[2] · Emilia Mariano[3] · E. Ng[2] · Antonio Del Prete[3] · Lars Nyborg[1]

Received: 7 February 2016 / Accepted: 6 June 2016 / Published online: 17 June 2016

Abstract It is well-known that the reliability of finite element (FE) simulation results of cutting processes depends mainly on two factors: implementation of a well-defined constitutive model which can properly represent the severe deformation in chip formation process as well as the viability of the relation adopted to simulate the frictional condition at the tool-chip interface. In the current study, a systematic approach is presented to evaluate the performance of various friction models in three different FE commercial codes: Deform 2D, Abaqus/Explicit and AdvantEdge. The frictional condition was analysed for two uncoated cemented carbide-plain carbon steel combinations: K10/AISI 1045 and H13A/AISI 1080. The results indicated that approximately similar ranges of minimum average error in simulation responses can be achieved, independently of the FE code used for simulation of the chip formation process and for both tool-work material combinations. The reasons for this observation were critically discussed.

Keywords Cutting process · Friction model · Finite element method · Artificial neural network · Johnson-Cook

✉ Amir Malakizadi
amir.malakizadi@chalmers.se

[1] Department of Materials and Manufacturing Technology, Chalmers University of Technology, 412 96 Gothenburg, Sweden

[2] Department of Mechanical Engineering, McMaster University, 1280 Main Street West, Hamilton L8S 4L7, Canada

[3] Department of Engineering Innovation, University of Salento, Via per Monteroni, 73100 Lecce, LE, Italy

1 Introduction

Metal cutting process often plays a central role in manufacturing industrial components, where they are closely dimensioned, new features such as holes and fillets are made and the specific demands on the properties of machined surfaces are secured. In cutting operations, the work material in the vicinity of the tool edge experiences a severe plastic deformation at very high strain rates, normally in order of 10^3–10^6 s^{-1}, and a substantial amount of heat is therefore generated at the tool-chip interface [1]. As a result, the tool edge is often subjected to high contact pressures and temperatures, the amounts of which can exceed 5 GPa and 1200 °C, respectively [1, 2]. Under such extreme conditions, the cutting edge can wear down after only a short machining time. The worn tools may in turn deteriorate the surface finish properties and the dimensional accuracy of the machined parts.

For many years, costly experimental procedures have been regarded as the only reliable method to estimate the tool life and to optimise the machining operations to achieve higher efficiency in terms of time and cost. In recent years, however, the significant advances in the computing power of computers have facilitated the application of advanced numerical techniques such as finite element method (FEM) in metal cutting research and development. This has provided the opportunity to simulate the responses such as tool surface temperature and stress distribution around the cutting edge under various cutting conditions and for different tool geometries, which in turn has allowed the development of cost-effective and robust approaches for tool wear estimations under operational conditions [3–5]. Yet, the reliability of the FE simulation results has shown to depend largely upon the reliability of the flow stress data to describe the severe plastic deformation in shear zone and viability of the frictional and thermal boundary conditions adopted at the tool-chip interface [6–8]. A vast number of

studies have been therefore dedicated to development of the experimental approaches such as Split Hopkinson Pressure Bar (SHPB) high strain rate test [9, 10] and inverse modelling of orthogonal cutting process [11–15] to determine the flow stress properties of the work material within the common range of strain, strain rate and temperature encountered during the chip formation process. In parallel, more advanced constitutive models have been proposed based on the experimental observations in order to represent the material behaviour under such extreme conditions [12, 16, 17].

The tribological conditions at the tool-chip interface have been studied using various experimental methods [18–22]. These studies have been generally aimed at understanding the tribological condition at contact regions and also development of an appropriate model that can represent the complex material deformation at the so-called secondary shear zone at the tool-chip interface. These methods involved the analysis of the frictional behaviour either directly by metal cutting tests or by tribometer instruments that can reproduce similar tribological conditions as the cutting process. A basic force analysis proposed by Merchant [23] was among the early attempts to assess the mean (apparent) friction coefficient based on the results of orthogonal cutting tests. This approach was extended by Usui et al. [24] using a more advanced slip-line field in the vicinity of the cutting edge to derive a universal expression for the mean Coulomb friction coefficient including the influence of rake angle and restricted contact length. In a more recent study, Atkins [25] presented a method to estimate the local frictional behaviour at the tool-chip interface based on the analysis of the cutting forces and the distribution of the normal stress along the contact length proposed by Zorev [26]. Tailored cutting experiments using the split and photoelastic tools have also been suggested by several authors [18, 19] to measure the local frictional condition on the rake face of the tools during chip formation process. Several attempts have also been made to develop tribometer instruments that can reproduce the tribological conditions at the tool-chip interface. For instance, Zemzemi et al. [20] and Rech et al. [21] redesigned the tribometer instrument proposed by Hedenqvist and Olsson [27] to achieve contact pressures as high as 3 GPa which can be considered within the common range of normal pressure on the rake face of the tools during chip formation process. Even though their approach ensured a reasonable range of contact pressure and interface temperature, the friction coefficient was measured on the non-fresh surfaces of the work material. To overcome this limitation, Smolenicki et al. [22] designed an in-process tribometer instrument that allowed to measure the friction coefficient on the newly generated non-oxidised pin-on-ring contact regions by pre-cutting the surfaces using a cutting tool placed at a small distance from the pin. Puls et al. [28] developed an experimental concept similar to the broaching equipment, where the clearance side of the tools was forced on thin sheets to induce local deformation in a range common in metal cutting. Under such conditions, the chip formation is suppressed as a result of a very negative rake angle and a uniform distribution of contact pressure is generated across the contact region. Accordingly, based on the observations of these experimental setups, several friction models have been proposed to describe the frictional condition in metal cutting process. The Coulomb (sliding) friction model [6, 9, 29–32], constant or variable shear friction relations [6, 11, 31, 33, 34], temperature or strain rate modified models [19, 28, 35] and finally the velocity-dependent Coulomb friction model [8, 20, 22] are the main relations presented in literature. The viability of these models has been investigated using FE commercial codes in a number of studies. Özel [6] compared the performance of a number of friction models adopted in Deform 2D FE commercial code. He showed that the variable friction models led the least deviations from the experimental measurements. Arrazola and Özel [36] used Abaqus/Explicit with Arbitrary Lagrangian-Eulerian (ALE) formulation to evaluate the performance of Coulomb friction model and sticking-sliding friction relation including various limiting shear stress values in simulation of orthogonal cutting process. It was shown that sticking-sliding shear friction model Abaqus/Explicit should be used with caution, as the acceptable values for limiting shear stress differ at various cutting conditions and they should therefore be adjusted carefully. Improper adjustments led to large simulation errors in terms of cutting forces and chip thickness. Bil et al. [31] compared the performance of three different FE commercial codes, MSC Marc, Deform 2D and AdvantEdge, with respect to the influence of friction coefficients, different remeshing criteria and threshold tool penetration values on the simulation results. The shear and sliding friction models with constant values were evaluated in their investigations. They showed that the FE simulation results depend significantly upon the friction coefficients. The lowest deviations in cutting force predictions were observed for smaller friction coefficients, whereas more accurate results were obtained for thrust force and shear angles using larger friction coefficients.

Apart from the study conducted by Bil et al. [31], the majority of investigations on viability of friction models have been limited to only one specific FE commercial code. Moreover, to the best of our knowledge, a systematic approach for evaluation of friction models has not been presented in previous studies. In the current study, the viability of the most widely used models for simulation of the frictional condition at the tool-chip interface has been evaluated. In addition, the performance of three different FE commercial codes, Deform 2D, Abaqus/Explicit and AdvantEdge, under nearly similar thermal and frictional boundary conditions has been investigated. In order to develop a systematic approach to evaluate the performance of friction models, the optimum sets of friction coefficients were initially determined, where the

criterion was set as the minimum average prediction error of all the simulated responses including the cutting force (F_C), feed force (F_f), chip thickness (CT) and the contact length (CL). The results indicated nearly a similar range of minimum average error for all the adopted friction models, independent of FE commercial code used for simulation of cutting process. The reasons for such behaviour were discussed critically, and the most viable models to represent the tribological condition at the tool-chip interface were identified.

2 Implemented friction models

The experimental stress measurements using split and photoelastic tools indicated two distinct contact zones on the rake face of the tools, widely referred to as sticking and sliding frictional zones. This has also been shown using other analysis techniques [37, 38]. In the sticking region, the friction stress is generally independent of the normal stress and is limited by the shear flow stress (k) of the work material. However, as the normal stress reduces on the rake face along the tool-chip contact length, the friction stress becomes proportional to the normal pressure (σ_n). This region on the rake face is referred to as the sliding zone. Shaw and his co-workers [39] characterised the sticking and sliding zones along the tool-chip interface based on the relation between the contact pressure and the real area of the contact (A_r), i.e. the total area of the asperities formed on the contact pair. According to this model, the frictional force between two contact surfaces is produced by the shearing action of the welded asperities, the amount of which supposedly varies with contact pressure as:

$$A_r = A_n[1-\exp(-\alpha\sigma_n)] \tag{1}$$

where A_n represents the apparent area of contact between the two surfaces and α is a constant. As evident from Eq. 1, the real contact area increases with an increase in the contact pressure, and it ultimately approaches the apparent area of contact at very high contact pressures. This state represents the sticking condition near the cutting edge, where the relative motion between the tool and chip material produces gross subsurface shear plastic deformation within the adhered material on the tool surface. However, as the contact pressure reduces along the tool-chip contact length, the real area of contact reduces. Under the condition where $A_r \ll A_n$, the shear friction stress becomes linearly proportional to the contact pressure, representing the sliding contact condition far from the cutting edge. The complex frictional condition at the tool chip-interface can therefore be formulated using a single mathematical relation with reference to Eq. 1, as also suggested by Childs [19] and Shirakashi and Usui [40]. The experimental data presented in literature [41] indicate that the shear friction stress in the sticking region may vary between $0.5k$ and k for different tool-work material combinations. The frictional behaviour is also shown to be highly nonlinear with respect to the variation of the contact pressure [41]. Hence, an additional parameter would be required to describe the shear friction stress within the entire range of contact pressure at the tool-chip interface:

$$\tau = \left[1-\exp\left(-\alpha_1\sigma_n^{\alpha_2}\right)\right]k \tag{2}$$

Figure 1a shows the variation of the friction coefficient with respect to the contact pressure for different combination of friction parameters. The local frictional behaviour at tool-chip interface may also be described using the following relation:

$$\tau = \begin{cases} \mu\sigma_n & \mu\sigma_n < mk \quad (L_{st} \le x \le L_{sl}) \\ mk & \mu\sigma_n \ge mk \quad (0 \le x \le L_{st}) \end{cases} \tag{3}$$

where L_{st} and L_{sl} represent the sticking and sliding contact lengths, respectively. μ and m are the sliding and sticking friction coefficients. Based on this model, the friction stress under sticking condition is proportional to the shear flow stress of the work material at tool-chip interface and it is proportional to the normal stress within the sliding zone. The

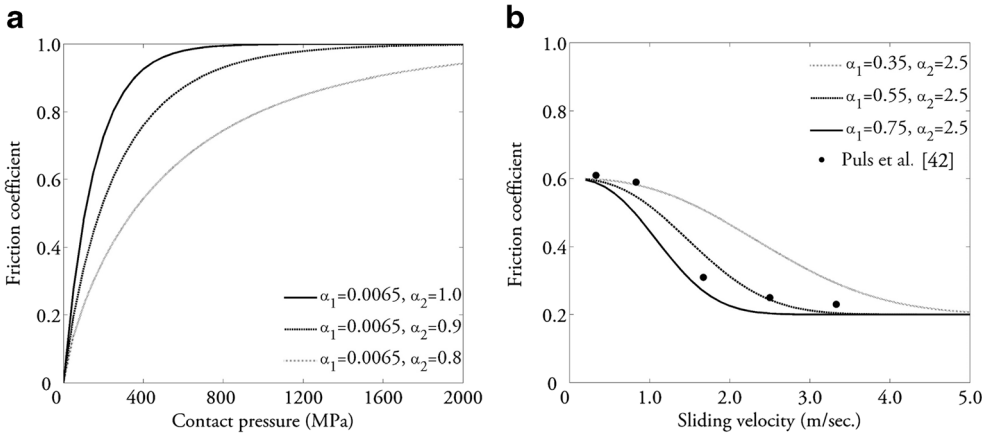

Fig. 1 Variation of pressure- and velocity-dependent friction coefficients with contact pressure and sliding velocity based on Eqs. 2 and 5, respectively. Experimental data for the velocity-dependent model were taken from Puls et al. [42]

Table 1 The friction models investigated in current study

Friction model	Mathematical formulation
Sliding friction model (SL) [7, 9, 29–32]	$\tau = \mu\sigma_n, \mu = \text{const.}$
Velocity-dependent friction model (VD)	$\tau = \mu\sigma_n, \mu = (0.6-\mu_0)\exp(-((\alpha_1 V_S)^{\alpha_2})) + \mu_0$
Shear friction model (SH) [6, 31, 33]	$\tau = mk, m = \text{const.}$
Pressure-dependent shear friction model (PD)	$\tau = mk, m = \left[1-\exp\left(-\alpha_1\sigma_n^{\alpha_2}\right)\right]$
Sticking-sliding friction model (SS) [6, 36, 43]	$\tau = \begin{cases} \mu\sigma_n & \mu\sigma_n < mk \quad (L_{st} \le x \le L_{sl}) \\ mk & \mu\sigma_n \ge mk \quad (0 \le x \le L_{st}) \end{cases}$

experimental measurements presented by Childs et al. [41] showed that the shear friction coefficient, m, may take a value between 0.5 and 1 while μ can take values as high as 1.5 when cutting steels using uncoated carbide tools. Both μ and m are also shown to vary significantly with temperature and contact pressure.

The Coulomb friction law has also been implemented to describe the shear stress at the tool-chip interface, assuming the friction coefficient as a function of either sliding velocity or interface temperature [8, 20]. Puls et al. [42] developed an experimental concept to provide the apparent Coulomb friction coefficient (μ_{app}) at various sliding velocities by measuring the axial and tangential forces acting on the clearance side of the tool while being forced in transverse direction toward the disc rotating in the opposite direction compared to the conventional case of a turning operation. In this way, it was possible to suppress the chip formation process as a result of a very negative rake angle (−80°) and therefore a uniform frictional condition could be reproduced across the contact region. The friction coefficient was then calculated based on the basic force analysis proposed by Merchant [23]:

$$\mu_{app} = \frac{F_t + \tan(\gamma)F_C}{F_C - \tan(\gamma)F_t} \tag{4}$$

where γ is the rake angle and F_t and F_C are the tangential and normal force across the contact region. In the current study, based on the results of this experimental setup, a mathematical relation was derived for the velocity-dependent Coulomb friction coefficient:

$$\mu = (0.6-\mu_0)\exp(-((\alpha_1 V_S)^{\alpha_2})) + \mu_0 \tag{5}$$

where α_1, α_2 and μ_0 are the model parameters. Here, μ_0 was assumed at 0.2, while the upper limit for friction coefficient was set at 0.6 based on the experimental measurements presented for H13A/AISI 1045 tool-work material combination [42]. Figure 1b shows the variation of the friction coefficient with sliding velocity for different combinations of parameters along with the experimental measurements.

Table 1 summarises the friction models adopted in the current study. In addition to Eqs. 2, 3 and 5, the Coulomb (sliding) and shear friction models with constant parameters were also adopted for simulation of the chip formation process. These models are often regarded as the standard relations for simulation of the tribological condition at tool-chip interface in metal cutting based on their availability in various FE commercial codes, as will be discussed in Section 3.2.

3 Evaluation methodology

In order to evaluate the viability of the presented friction models to describe the frictional condition at the tool-chip

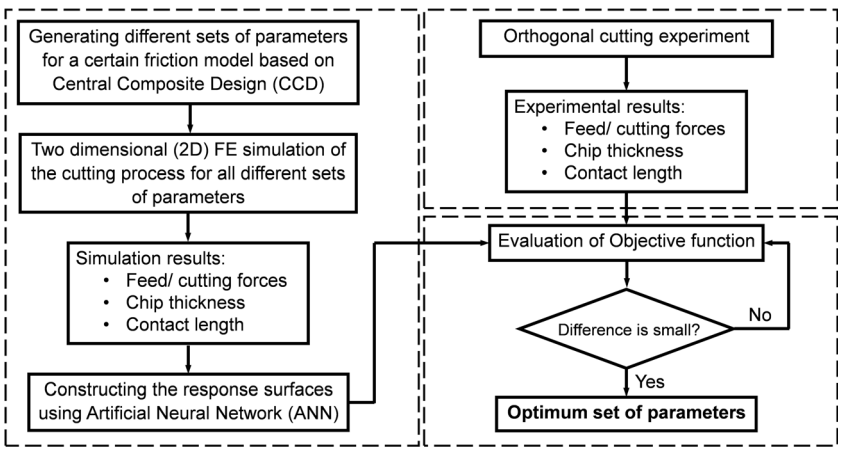

Fig. 2 The flowchart indicating the steps of the evaluation methodology adopted in this study

Table 2 The lower and upper bounds of the friction parameters adopted in the current study

Friction model	Lower bound	Upper bound	Number of combinations
Sliding friction model (SL)	$\mu = 0.2$	$\mu = 0.6$	3
Velocity-dependent friction model (VD)	$\alpha_1 = 0.35$, $\alpha_2 = 0.5$	$\alpha_1 = 0.75$, $\alpha_2 = 2.5$	9
Shear friction model (SH)	$m = 0.5$	$m = 1.0$	3
Pressure-dependent shear friction model (PD)	$\alpha_1 = 0.0025$, $\alpha_2 = 0.8$	$\alpha_1 = 0.0065$, $\alpha_2 = 1.0$	9
Sticking-sliding friction model (SS)	$\mu = 0.2$, $m = 0.5$	$\mu = 0.6$, $m = 1.0$	9

interface, initially the optimum combination of friction parameters was determined for each model according to the steps shown in Fig. 2. The aim was to ensure that the friction models were evaluated based on their optimum combinations at which the least deviations from the experimental measurements, including the chip thickness, contact length and the cutting/feed forces, were achieved. This allowed for a more systematic evaluation of the performance of a certain friction model by calculation of the percentage of the average simulation errors.

As evident from Fig. 2, initially a different combination of friction parameters was generated for each of the models presented in Table 1. In the case of the models with two parameters (i.e. VD, PD and SS models), the central composite design (CCD) was adopted to generate nine different combinations of friction parameters in three levels. The friction coefficient for the models with only one parameter was also varied in three levels; however, the step sizes were set similar as the ones adopted in the sticking-sliding model. The chip formation process was then simulated in different FE commercial codes incorporating various combinations of friction parameters generated for each model. Two different cutting conditions, A and C, were simulated in this step for both tool/material combinations (see Table 3). The response surfaces were then established for models with two parameters using artificial neural network (ANN) platform available in MATLAB software [45] to describe the relation between friction parameters and the simulated outputs. In the case of the models with only one parameter (e.g. sliding friction (SL) and shear friction (SH) models), the mathematical relations between the friction coefficient and the simulation outputs were simply expressed as third-order polynomials. The optimum sets of friction coefficients were then identified by formulating an optimisation problem as:

$$\mathrm{Min}\, f(x)\, such\, that\, X_{\mathrm{lb}} < X < X_{\mathrm{ub}} \tag{6}$$

where X_{lb} and X_{ub} represent the vectors including the lower and upper bounds of the friction parameters for a certain model. Table 2 shows the upper and lower bounds set for each of the friction model as well as the total number of variations adopted for each model to determine the response surfaces (or the third-order polynomials). Note that the upper and lower values of the Coulomb friction model (SL) were set based on the experimental data presented by Puls et al. [42] for H13A-AISI 1045 tool-workpiece material combinations. $f(X)$ in Eq. 6 represents the objective function expressed as:

$$f(X) = \sum_{m=1}^{4} \left\{ w_m \left[\sum_{n=1}^{N} \left(\frac{Y_{mn,\mathrm{ANN}} - Y_{mn,\mathrm{EXP}}}{Y_{mn,\mathrm{EXP}}} \right)^2 \right] \right\} \tag{7}$$

where X is a vector including the friction parameters. N is the number of cutting conditions used for identification of optimum friction coefficients. $Y_{mn,\mathrm{ANN}}$ and $Y_{mn,\mathrm{EXP}}$, respectively, represent the calculated responses by integration of FEM and ANN and the corresponding experimental measurements at similar cutting conditions. w_m is the weight factor for each term in Eq. 7, and they were assumed unitary in the current study to ensure an identical impact for each term in the objective function in the optimisation process. The interior point optimisation

Table 3 The cutting data used in the current study

Work material	Condition	Tool material	Cutting speed (m/min)	Rake angle (°)	Feed rate (mm/rev)	Depth of cut (mm)
AISI 1080	A	H13A	90	0	0.1	2
	B		120			
	C		180			
AISI 1045 [44]	A	K10	120	6	0.1	NA[a]
	B		120		0.2	
	C		240		0.1	
	D		240		0.2	

[a] Depth of cut at least 10 times larger than uncut chip thickness [44]

Table 4 The experimental measurements during orthogonal machining AISI 1080 and AISI 1045 steels

Work material	Condition	CT (mm)	CL (mm)	F_C (N/mm)	F_f (N/mm)
AISI 1080 [11]	A	0.279	0.524	278	226
	B	0.244	0.425	263	197
	C	0.219	0.423	267	180
AISI 1045 [44]	A	0.320	1.000	287	259
	B	0.500	1.325	459	302
	C	0.290	0.725	234	179
	D	0.450	1.089	413	224

algorithm with multiple starting points in MATLAB was adopted to find the global optimum solution.

3.1 Material and experimental details

The orthogonal machining tests for AISI 1080 eutectoid steel were performed under dry condition using Sandvik N151.2-650-50-3B-H13A standard uncoated cemented carbide [11]. Prior to machining tests, a cylindrical bar with 60 mm diameter and 55 mm length was heat treated to achieve a pearlitic structure with fine lamellar spacing. The procedure involved initial austenitisation at 865 °C for 1 h followed by 10 min cooling within a salt bath with 590 °C and air cooling to room temperature. The heat treatment procedure resulted in a fully pearlitic structure with 0.274-μm mean true lamellar spacing. All machining tests were performed on an EMCO 365 CNC lathe equipped with a Kistler 9275A three-component dynamometer to measure the cutting forces. Orthogonal cutting condition was met through transverse machining of flanges with 2-mm thickness, generated on the cylinder prior to machining tests. Each cutting test was repeated three times with fresh inserts to ensure reproducibility of the experimental results.

A Leitz DMRX light optical microscope equipped with AxioVision digital image processing software was used to measure the thickness of randomly selected chips produced under various cutting conditions. The chip-tool contact lengths were also measured by means of energy-dispersive spectroscopy (EDS) analysis on the rake face of the inserts after machining using iron elemental mapping.

The experimental data for AISI 1045 alloy were taken from [44]. The author used K10 uncoated carbide with 6° rake angle and no chip breaker for orthogonal cutting tests. The orthogonal cutting tests were performed on tubes with cutting width at least ten times larger than the feed rates. Table 3 shows the cutting conditions used in the current study for evaluation of the friction models. Table 4 shows the experimental measurements.

3.2 Finite element modelling of cutting process

The chip formation process in Deform 2D and AdvantEdge was simulated using Lagrangian formulation, while the FE models in Abaqus/Explicit were constructed using ALE formulation. Figure 3 shows the adopted structural boundary conditions for the FE models based on ALE and Lagrangian formulations. In ALE approach, the mesh around the cutting edge, where the work material undergoes severe plastic deformation, is fixed in space and it follows the Eulerian formulation. However, the mesh at the machined surface and also within the part of the work material which forms the final geometry of the chip is left unconstrained and follows Lagrangian formulation. Hence, the elements on the chip tail are steadily expanded and the final chip is produced during FE

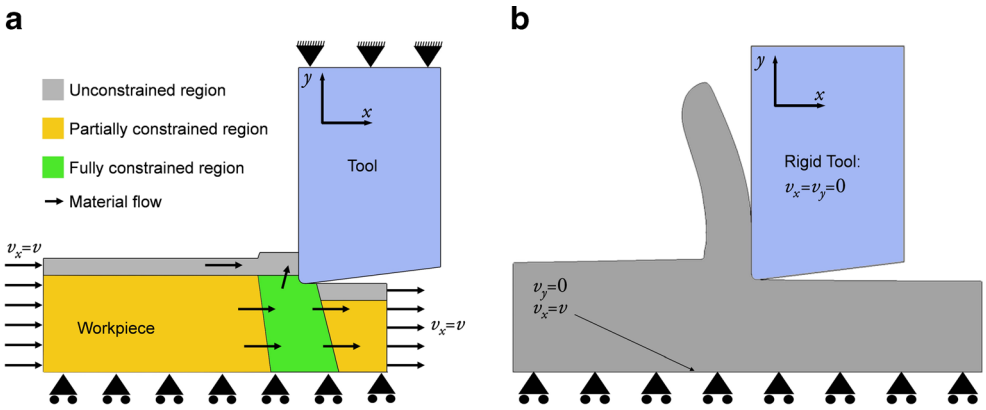

Fig. 3 The boundary conditions adopted for ALE (**a**) and Lagrangian (**b**) FE models

Table 5 The Johnson-Cook material parameters for AISI 1045 [44] and AISI 1080 [11]

Material	A	B	C	n	m	$\dot{\varepsilon}_0$	T_m (K)
AISI 1045	553.1	600.8	0.0134	0.234	1	1	1773
AISI 1080	534.6	410	0.0062	0.137	1.01	1	1738

analysis. The chip separation in Deform 2D and AdvantEdge is undertaken by continuous remeshing to eliminate the distorted elements during the analysis [31, 46]. Once the new mesh is generated, the calculated outputs from the step prior to the remeshing stage are interpolated on the new mesh. The details of ALE and Lagrangian formulations adopted for FE modelling of the cutting process can be found in [33, 47].

The tool in Deform 2D was assumed to be rigid due to its relatively high elastic modulus, while the elastic properties of the tool were directly included in the FE model built in Abaqus/Explicit and AdvantEdge. Johnson-Cook constitutive model was incorporated in all FE codes to simulate the visco-plastic behaviour of the work material within the range of strain, strain rate and temperature encountered during the chip formation process:

$$\sigma = (A + B\varepsilon^n)\left[1 + C\ln\left(\frac{\dot{\varepsilon}}{\dot{\varepsilon}_0}\right)\right]\left[1-\left(\frac{T-T_r}{T_m-T_r}\right)^m\right] \quad (8)$$

In this model, σ is the flow stress of the work material, ε is the strain, T is the temperature and $\dot{\varepsilon}$ is the strain rate. A, B, C, n and m represent the material parameters. $\dot{\varepsilon}_0$ is the reference strain rate and T_m and T_r represent the melting and room temperatures, respectively. The constitutive data for AISI 1045 were taken from [44], where the author used SHPB high strain rate test for calibration of the Johnson-Cook material model. In the case of AISI 1080, the material parameters were obtained using inverse modelling of orthogonal cutting process [11]. In this approach, the author combined response surface methodology (RSM) and Oxley's machining theory to determine the mathematical relation between the material parameters and the outputs of interests including the feed force, cutting force, chip thickness and contact length for a certain cutting data. The optimum set of material parameters were then identified by minimising the difference between the estimation of the outputs based on the established mathematical relations and the corresponding experimental measurements at similar cutting conditions. Table 5 shows the material parameters of the Johnson-Cook model incorporated in this study for AISI 1045 and AISI 1080. The thermal properties of the tool and work-piece material are also shown in Table 6. The temperature-dependent data for AISI 1045 were taken from [48], while JMatPro™ commercial software [50] was used to obtain the thermal properties for AISI 1080.

Table 7 The friction models adopted in different FE codes in the current study

FE code	VD	PD	SL	SH	SS
Deform 2D	✓	✓	✓	✓	✓
AdvantEdge	–	–	✓	–	–
Abaqus/Explicit	✓	–	✓	–	–

As mentioned before, AdvantEdge FE commercial code only supports the Coulomb friction model (SL) with constant values. In addition to the standard Coulomb friction model, it is also possible to provide the velocity-dependent Coulomb friction coefficients in Abaqus/Explicit using tabulated data. Hence, both the constant and velocity-dependent friction models were implemented for FE modelling of the cutting process using Abaqus/Explicit. A wider range of friction models including the Coulomb, shear and sliding-sticking friction models are available in Deform 2D, where the friction coefficients can be defined either as a constant or as a function of temperature and/or pressure using tabulated data. In addition, Deform 2D provides a platform to adopt a user-defined friction coefficient as a function of temperature, shear flow stress, contact pressure and sliding velocity for each of the aforementioned friction models by developing FORTRAN sub-routines. In this study, the velocity and pressure-dependent friction models presented in Table 1 were implemented using this platform. Table 7 shows the summary of the friction models implemented in different FE codes in the current study.

Table 6 The thermal properties of the tool and work materials

Material	λ (W/m K)	$\rho \times C_p$ (J/cm^3 K)
AISI 1045 [48]	25 °C < T < 600 °C: $3.91\times10^{-8}T^3-4.74\times10^{-5}T^2-0.0121T+46.1$	25 °C < T < 600 °C: $4.685\times10^{-6}T^2+1.527\times10^{-3}T+3.664$
	T > 600 °C: 26	T > 600 °C: 6.28
AISI 1080 [11]	25 °C < T < 900 °C: $4\times10^{-8}T^3-4\times10^{-5}T^2-0.0195T+50.32$	25 °C < T < 900 °C: $9\times10^{-7}T^2+0.0022\ T+3.735$
H13A [11]	25 °C < T < 1000 °C: $6\times10^{-8}T^3-9\times10^{-5}T^2-0.0083T+94.834$	25 °C < T < 1000 °C: $3\times10^{-9}T^3-5\times10^{-6}T^2+0.0041T+2.886$
K10 [49]	80	5.7

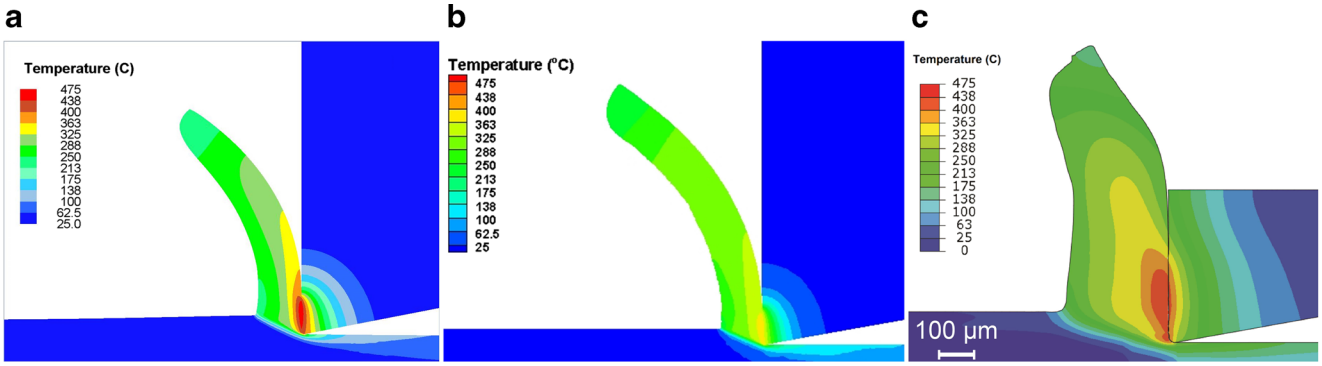

Fig. 4 Calculated temperature distribution in the vicinity of tool edge at cutting condition B using Deform 2D (**a**), AdvantEdge (**b**) and Abaqus/Explicit (**c**). Work material: AISI 1080, Coulomb friction model, COF = 0.4

Perfect thermal condition was assumed at tool-chip interface in Deform 2D and Abaqus/Explicit. This was achieved by adjusting a very heat transfer coefficient and high gap conductance at the tool-chip contact surfaces in the FE models. The ideal thermal condition at the tool-chip interface has been widely accepted for the simulation of cutting process [32, 43, 51], which has been experimentally verified for a number of tool-work material combinations through temperature measurements [52, 53]. The AdvantEdge FE commercial code, however, does not take into account the heat conduction between the tool and work material, and therefore, it is not possible to adjust interface properties as such in the FE models. Furthermore, a different partitioning assumption has been made in Deform 2D, Abaqus/Explicit and AdvantEdge FE codes to apportion the heat due to frictional work between the tool and chip material. Deform 2D and AdvantEdge commercial codes adopt predefined values to divide the generated heat between the tool and chip, whereas it is possible to adjust the heat partitioning coefficient in Abaqus/Explicit for the frictional contacts. AdvantEdge adopts the approach proposed by Sekhon and Chenot [54] to compute the ratio of heat supply to the tool and chip [46]. A similar approach was also followed to calculate the heat partitioning coefficient for FE models in Abaqus/Explicit [30]. The generated heat through friction is, however, evenly distributed between the tool and chip in Deform 2D. These differences in FE formulations and thermal boundary conditions should be taken into account while comparing the FE simulation results.

4 Evaluation of simulation results

Figures 4 and 5 show the FE simulation results of the chip formation process, indicating the temperature distribution in the vicinity of the cutting edge for AISI 1080 and AISI 1045 carbon steels at cutting conditions B and D, respectively, using Deform 2D, AdvantEdge and Abaqus/Explicit FE commercial codes. In all cases, the Coulomb friction model with a constant friction coefficient of 0.40 was adopted for FE modelling of the cutting process. Figure 6 summarises the other simulated responses at the corresponding cutting conditions for each material. As evident from these figures, a similar frictional condition led to different simulation results in various FE codes.

Figure 7 shows the established response surfaces by ANN based on the FE simulation results of the cutting process, incorporating the pressure-dependent shear friction model (PD), for AISI 1080 carbon steel at cutting condition A. As

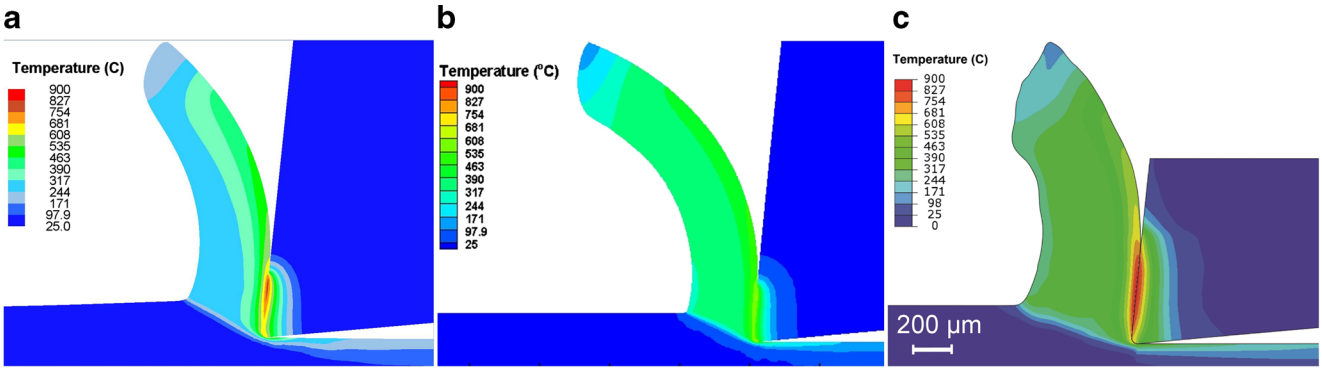

Fig. 5 Calculated temperature distribution in the vicinity of tool edge for cutting condition D using Deform (**a**), AdvantEdge (**b**) and Abaqus/Explicit (**c**). Work material: AISI 1045, Coulomb friction model, COF = 0.4

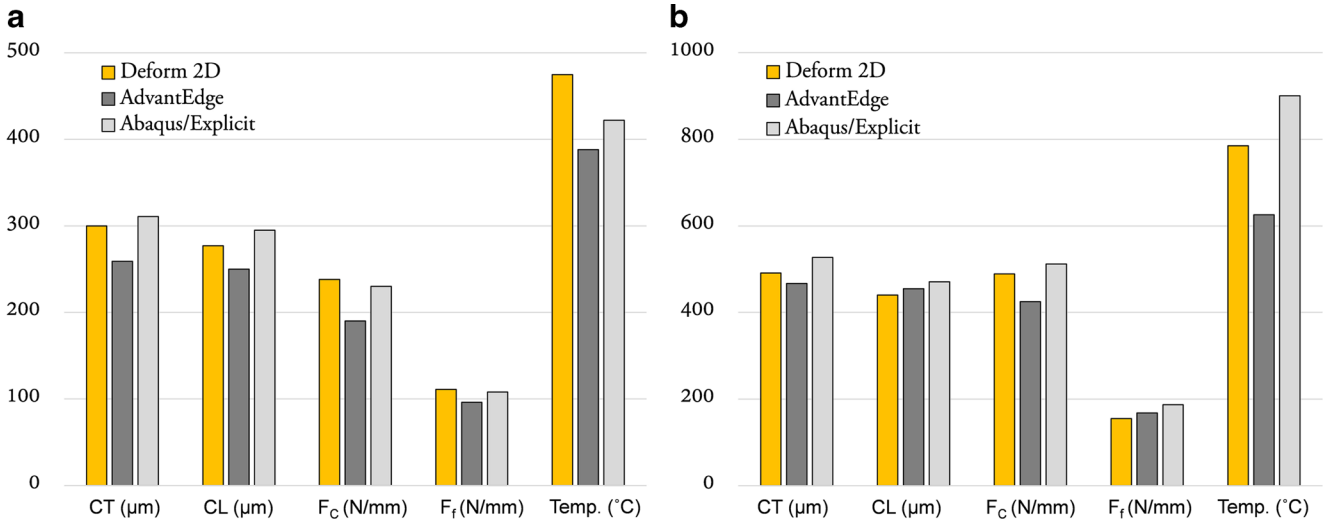

Fig. 6 Summary of the FE simulation results of the chip formation process using different FE codes for AISI 1080 at cutting condition B (**a**) and AISI 1045 at cutting condition D (**b**), Coulomb friction model, COF = 0.4

evident, different combinations of the friction parameters give rise to the varying simulation results; however, the degree of variation differs for each response. Figure 8 also shows the simulated cutting and feed forces for AISI 1045 plain carbon steel at cutting condition A, using the adopted velocity-dependent friction model in Deform 2D and Abaqus/Explicit. Evidently, the FE simulation results substantially varied between different FE codes. In addition, the maximum response was achieved at different combinations of friction parameters. For instance, the maximum cutting and feed

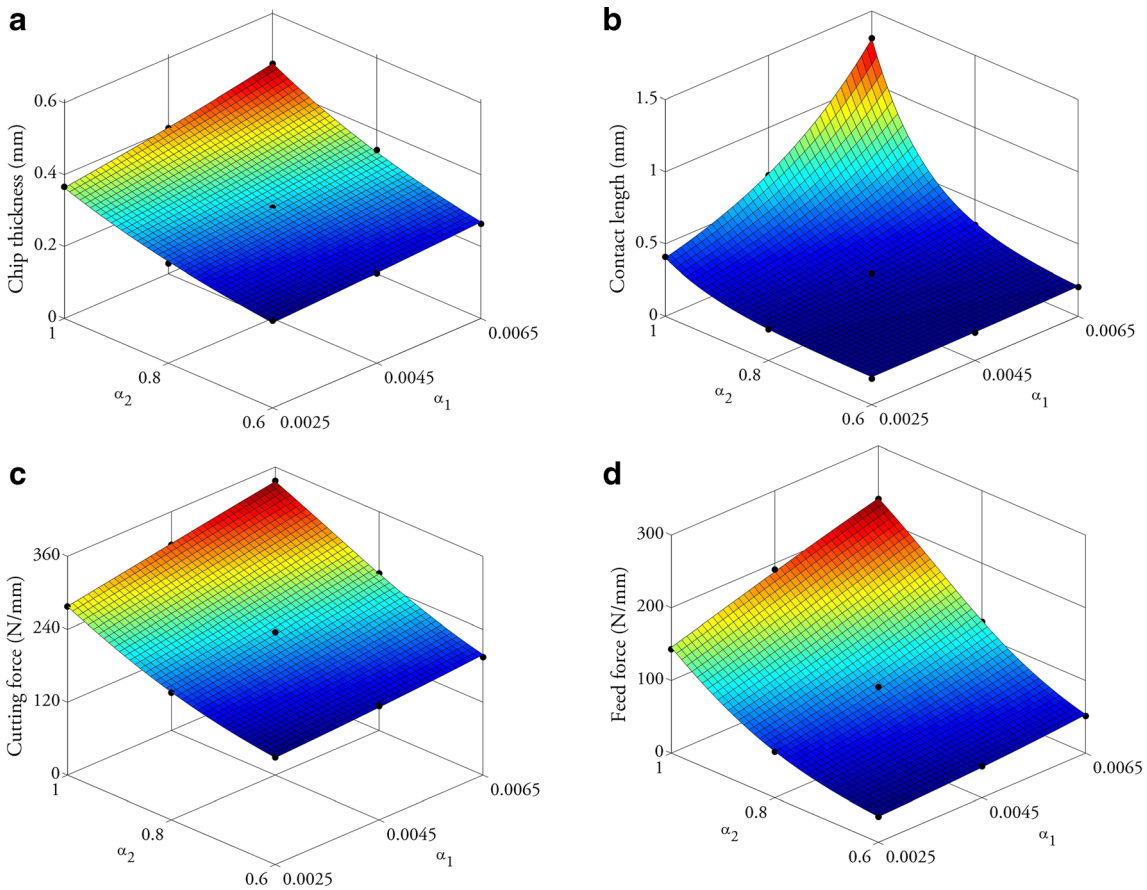

Fig. 7 The influence of the pressure-dependent (PD) friction model parameters on chip thickness (**a**), contact length (**b**), cutting force (**c**) and feed force (**d**): AISI 1080 at cutting condition *A*

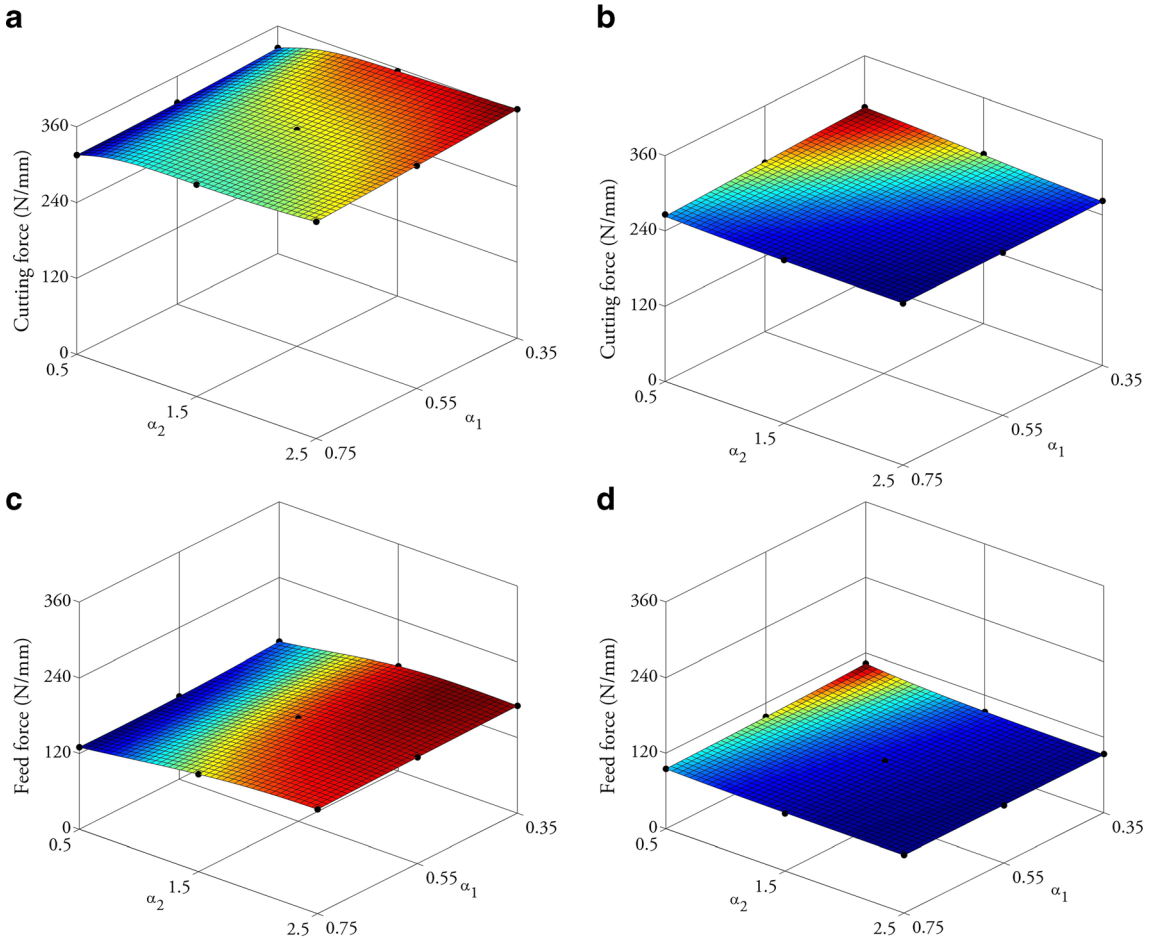

Fig. 8 The influence of the parameters of the velocity-dependent (VD) friction model implemented in Deform 2D (**a** and **c**) and Abaqus/Explicit (**b** and **d**) FE commercial codes on cutting and feed forces for AISI 1045 at cutting condition A

forces were observed at (α_1, α_2) = (0.35, 2.5) and (α_1, α_2) = (0.35, 0.5) when modelling the cutting process in Deform 2D and Abaqus/Explicit, respectively. It should be noted, however, that the variations in the FE simulation results were relatively small in Abaqus/Explicit between different combinations of friction parameters, as can be seen in Fig. 8b, d.

The optimum sets of friction coefficients were obtained by implementation of the methodology shown in Fig. 2. The results are summarised in Tables 8 and 9 for the investigated tool/work material combinations. The error in the simulated responses after implementation of the optimum sets of friction parameters in FE models is also shown in Figs. 9, 10, 11 and 12 for AISI 1045 at cutting conditions A and B and AISI 1080 at cutting conditions B and C.

5 Discussion

The methodology presented in the current study provided a more systematic evaluation of the friction models compared to the previous attempts, where often the error in feed force predictions was considered as the main factor for the assessment of the viability of the adopted friction models [6, 8]. In the

Table 8 The optimum sets of friction parameters obtained for K10/AISI 1045 tool-work material combinations within the range of DOE given in Table 2

Friction model	Deform 2D	Abaqus/Explicit	AdvantEdge
Sliding friction model (SL)	$\mu = 0.6$	$\mu = 0.6$	$\mu = 0.6$
Velocity-dependent friction model (VD)	$\alpha_1 = 0.44$, $\alpha_2 = 2.26$	$\alpha_1 = 0.35$, $\alpha_2 = 0.5$	–
Shear friction model (SH)	$m = 0.83$	–	–
Pressure-dependent shear friction model (PD)	$\alpha_1 = 0.0065$, $\alpha_2 = 0.92$	–	–
Sticking-sliding friction model (SS)	$\mu = 0.6$, $m = 1.0$	–	–

Table 9 The optimum sets of friction parameters obtained for H13A/AISI 1080 tool-work material combinations within the range of DOE given in Table 2

Friction model	Deform 2D	Abaqus/Explicit	AdvantEdge
Sliding friction model (SL)	$\mu = 0.6$	$\mu = 0.4$[a]	$\mu = 0.6$
Velocity-dependent friction model (VD)	$\alpha_1 = 0.75$, $\alpha_2 = 2.5$	$\alpha_1 = 0.35$, $\alpha_2 = 0.73$	–
Shear friction model (SH)	$m = 0.79$	–	–
Pressure-dependent shear friction model (PD)	$\alpha_1 = 0.0065$, $\alpha_2 = 0.88$	–	–
Sticking-sliding friction model (SS)	$\mu = 0.6$, $m = 1.0$	–	–

[a] FE simulations did not reach the thermal steady state condition for the larger friction coefficients after 5 mm of cut

current approach, on the contrary, the optimum friction parameters were initially determined for each model by adjusting an identical impact for all the responses under investigation during the optimisation process. Evaluation of the FE simulation results utilising the optimum sets of parameters indicated that the performance of the friction models in terms of the average prediction error of all investigated responses was nearly identical for K10/AISI 1045 tool-work material combination, although the adopted pressure-dependent shear friction model in Deform 2D resulted in a slightly smaller percentage of the average error. This is due to the fact that the distribution of the error between the simulated responses varies by implementation of different friction models. Hence, for instance, while the pressure-dependent shear friction model implemented in Deform 2D resulted in the least deviation from the experimental measurements of contact length and feed force for K10/AISI 1045 tool-work material combination at both cutting conditions, larger deviations were attained for the cutting force and chip thickness compared to the other adopted friction models. Therefore, the calculated average error becomes nearly identical for all friction models. As can be seen in Figs. 9, 10, 11 and 12, the distribution of the error between the simulated responses also varies for a certain friction model (e.g. sliding friction model) adopted in different FE codes. This perhaps stems from the differences in FE formulations in terms of the element type definition, thermo-mechanical coupling and the assumptions associated with the adaptive remeshing and ALE formulations in various FE codes. However, certain patterns can still be noted in the distribution of the error between the simulated responses. For instance, all FE models underestimated the feed force and the tool-chip contact length for the K10/AISI 1045 tool-work material combination, while the cutting force and the chip thickness were overestimated in most cases. On the other hand, for H13A/AISI 1080 tool-work material combination, the FE models only overestimated the chip thickness at both cutting conditions, independent of the FE code and the friction model used for simulation chip formation process. However, the calculated average errors in this case are typically smaller than those of K10/AISI 1045 tool/work material combinations shown in Figs. 9 and 10. This perhaps reflects the importance of the implementation of a well-defined constitutive model to describe the material deformation within the common range of strain, strain rate and temperature encountered in metal cutting process. As noted in Section 3.2, the JC material parameters for the AISI 1080 carbon steel were obtained using inverse

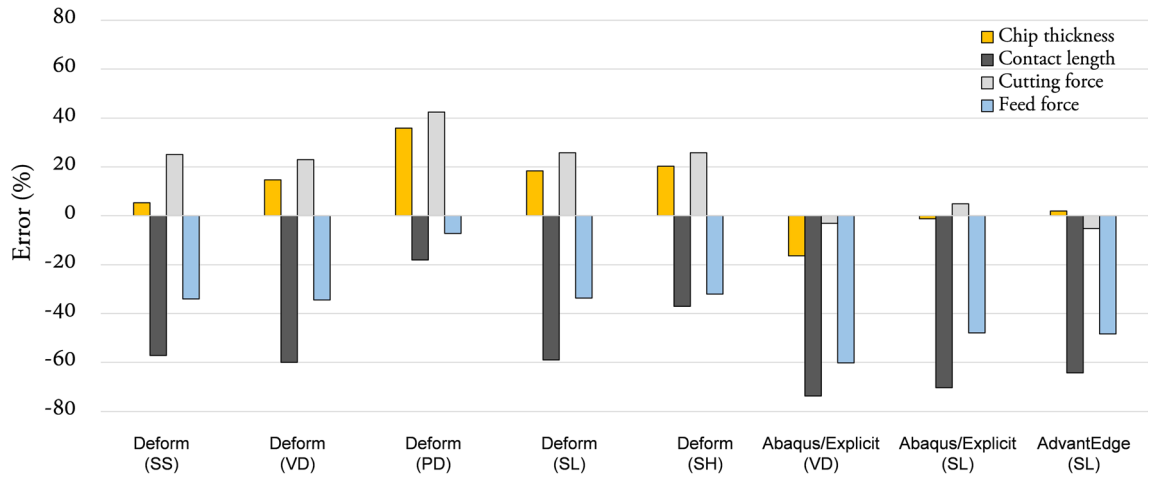

Fig. 9 The error percentage in simulated responses using different FE codes and friction models: AISI 1045, cutting condition A. The experimental results given in Table 4 were considered as the reference

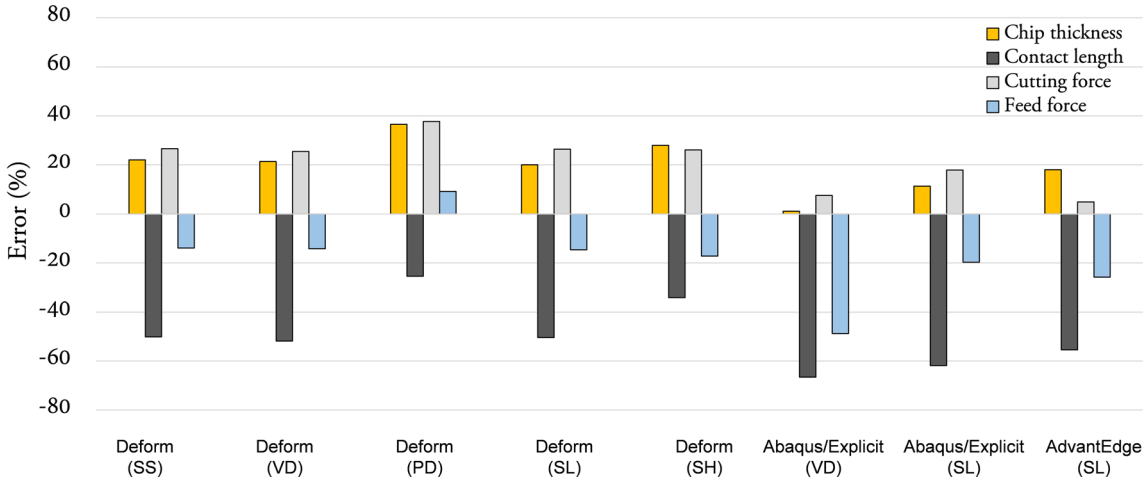

Fig. 10 The error percentage in simulated responses using different FE codes and friction models: AISI 1045, cutting condition B. The experimental results given in Table 4 were considered as the reference

modelling of the orthogonal cutting process, which can perhaps better represent the material deformation during the chip formation process. The importance of a well-defined constitutive model to achieve reliable FE simulation results has also been stressed by other authors [19]. Özel [6] and Iqbal et al. [55] investigated the viability of various friction models to describe the frictional condition at the tool-chip interface. Özel [6] reported that the implementation of the variable shear friction model can significantly improve the feed force predictions; however, up to 50 % error in cutting force estimations was still noted at various ranges of the cutting speeds. Iqbal et al. [55] showed that a realistic definition of the sticking-sliding contact lengths determined by SEM-EDX analyses of the contact region [38] on the rake face of the tools can enhance the reliability of FE simulation results. Yet, the authors reported as high as 30 % error in cutting force predictions, despite a more realistic description of the sliding-sticking contact regions in the FE models. It was therefore concluded that the simulation errors cannot be further reduced, unless an appropriate constitutive model with well-defined parameters is adopted for FE simulation of chip formation process. A similar conclusion can be made by evaluation of the results in the current study, see for instance the calculated error percentage presented in Figs. 9, 10, 11 and 12 for the optimum sets of friction coefficients. Nevertheless, one may still critically discuss the viability of the friction models and the ranges of friction parameters adopted in the current study to represent the frictional condition at the tool-chip interface regardless of the influence of the constitutive model and FE formulations implemented for simulation of chip formation process. As mentioned in Section 2, the velocity-dependent Coulomb friction model (VD) in this study was derived based on the experimental data of a tailored tribometer test presented by Puls et al. [42]. The apparent Coulomb friction coefficient

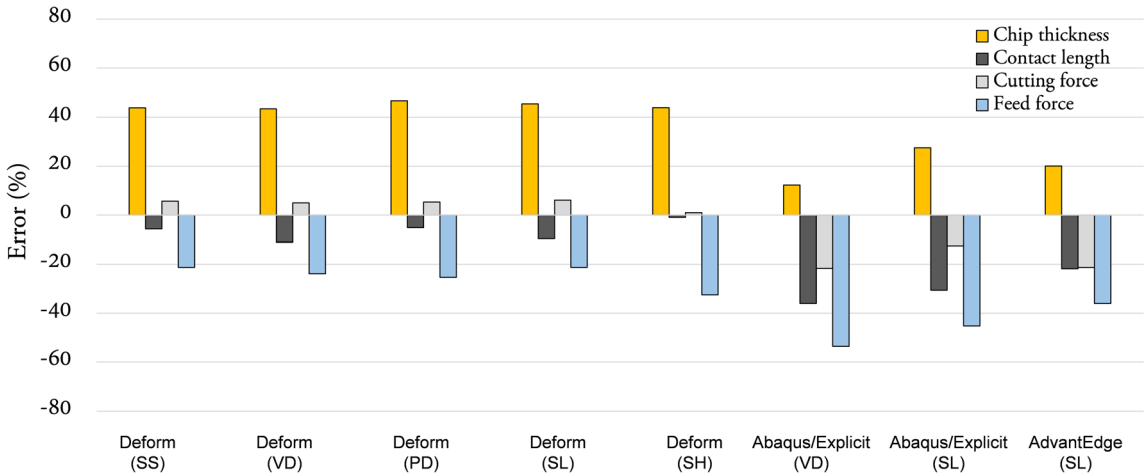

Fig. 11 The error percentage in simulated responses using different FE codes and friction models: AISI 1080, cutting condition B. The experimental results given in Table 4 were considered as the reference

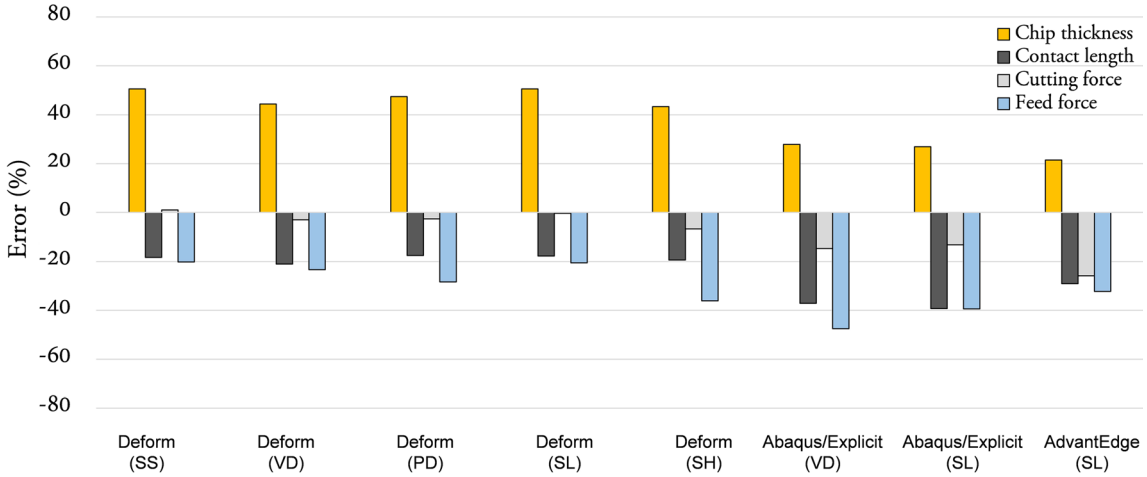

Fig. 12 The error percentage in simulated responses using different FE codes and friction models: AISI 1080, cutting condition C. The experimental results given in Table 4 were considered as the reference

measured by the authors varied between 0.6 and 0.2 with increasing sliding velocity from 25 to 200 m/min. It should be noted that this range of Coulomb friction coefficient has been widely accepted for FE modelling of the cutting process [30, 56, 57]. A similar range of friction coefficient was therefore adopted in the current study to evaluate the performance of the Coulomb friction (SL) model. However, as depicted in Fig. 13, the calculation of the mean (apparent) friction coefficient based on the orthogonal cutting force analysis presented by Merchant [23] (see Eq. 4) suggests a significantly larger values for K10/AISI 1045 tool-work material combination. Furthermore, as evident from Fig. 13, the mean friction coefficient varied with both feed rate and the cutting speed. Similar analyses by Merchant [23], Zorev [26], Usui et al. [24] and Bailey [58] showed that, in general, the mean friction coefficient in metal cutting varied with feed rate, cutting speed, the tool rake angle and the presence of lubrication. As shown by Usui et al. [24] and more recently by Atkins [25], the variation in the mean friction coefficient is, in fact, due to the variation in the relative proportion of sticking-sliding friction zones with the cutting parameters and the tool geometry. Obviously, such frictional behaviour cannot be fully reproduced by the tribometer tests and hence the measured values of the mean friction coefficient by those instruments may not represent the frictional condition within the entire range of cutting data and for all different tool geometries. The additional limitation of the tribometer test data is that the influence of sliding velocity and interface temperature on the measured mean friction coefficients cannot be easily separated, and therefore, it is difficult to evaluate.

Figure 14 shows the variation of the velocity-dependent friction coefficient (Eq. 5) as well as the estimated sliding velocity and the interface temperature along the contact length for H13A/AISI 1080 at cutting conditions B and C (see Table 3). As evident, the FE simulation results suggested that the sliding velocity increases along the contact length from zero near the cutting edge to nearly one third of the cutting speed (i.e. $V_{S,Max} \approx 1/3V_C$) as the chip leaves the rake face of the tool, while the interface temperature passes through its maximum in the middle of the contact region. In tribometer tests, however, the interface temperature and sliding velocity are directly proportional, i.e. with an increase in the sliding velocity, the interface temperature increases. Hence, the mean friction coefficient obtained by tribometer instruments and the

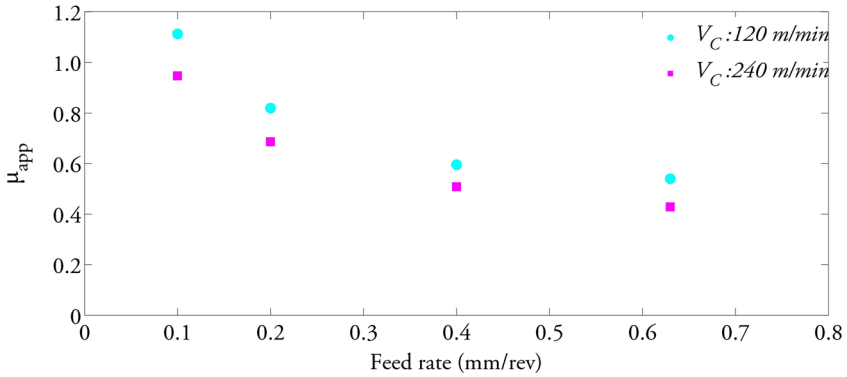

Fig. 13 The variation in mean friction coefficient with feed rate and cutting speed calculated using Merchant [23] analysis of orthogonal cutting/feed force data provided by Jaspers [44] for K10/AISI1045 tool-work material combination

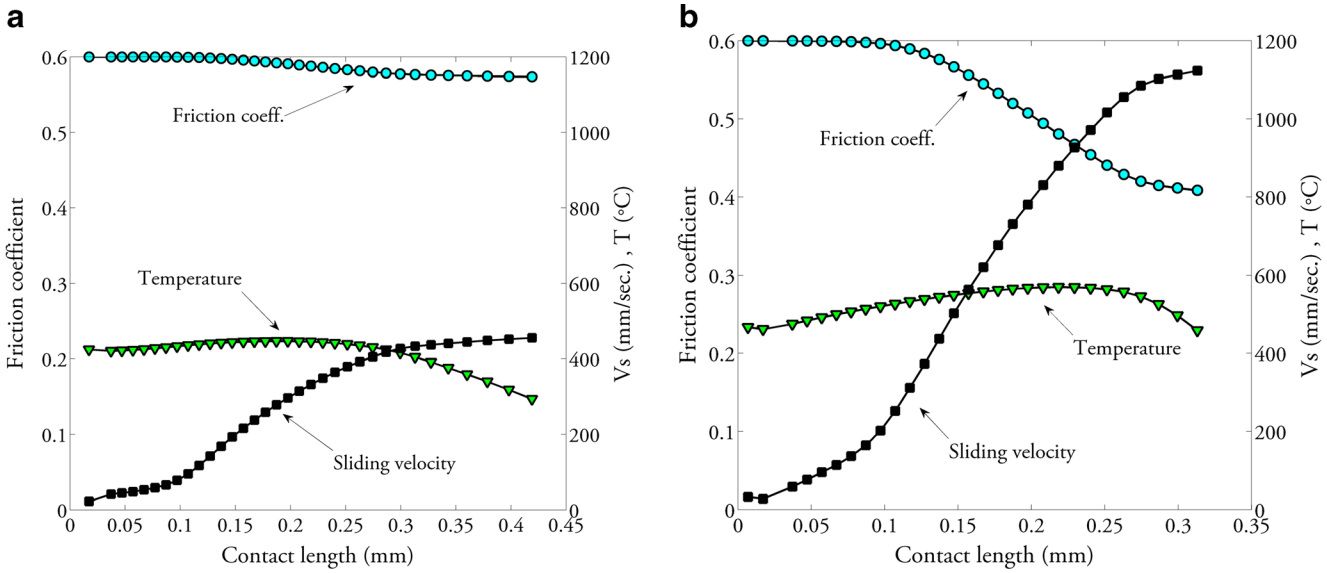

Fig. 14 The variation of velocity-dependent (VD) friction coefficient together with sliding velocity along the contact length: AISI 1080, cutting conditions B (**a**) and C (**b**). The process was simulated using Deform FE code

mathematical expression in the form of Eq. 5 may not fully express of the tribological condition on the tool-chip interface.

In light of these considerations, the sliding-sticking and pressure-dependent shear friction models are perhaps the most physically relevant expressions to describe the frictional condition at the tool-chip interface. Figure 15 shows the variation in pressure-dependent shear friction coefficient as well as the predicted normal and shear stresses along the contact length. As evident, the shear friction coefficient reduces with decreasing the normal pressure according Eq. 3. On the other hand, the shear strength of the work material varies with the strain, strain rate and temperature along the contact length according to the implemented constitutive model. Hence, in addition to the normal pressure, this model includes the influence of temperature and material deformation on the friction stress along the contact length in an indirect manner. As mentioned earlier, however, further improvement in prediction results is solely possible if a more viable constitutive model is adopted to describe the severe material deformation during the chip formation process.

6 Conclusions

In the current study, a systematic approach was presented to evaluate the performance of various friction models in FE

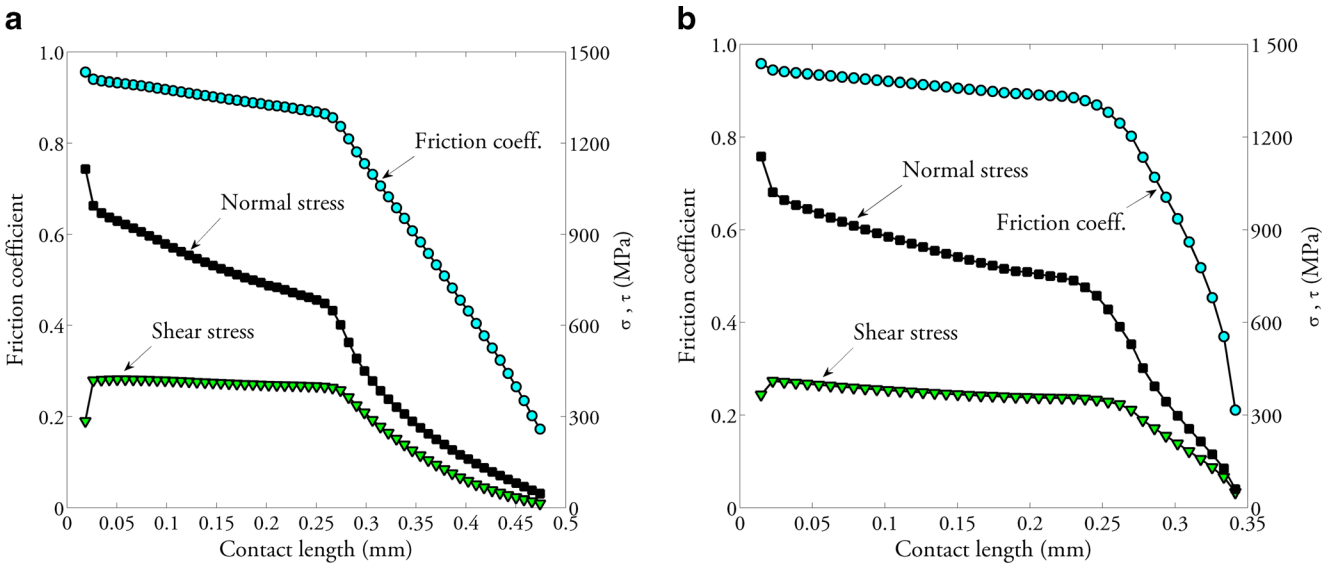

Fig. 15 The variation of pressure-dependent (PD) shear friction coefficient as well as the normal and shear stress along the contact length: AISI 1080, cutting conditions B (**a**) and C (**b**). The process was simulated using Deform FE code

simulation of the orthogonal cutting process using three different FE commercial codes: Deform 2D, Abaqus/Explicit and AdvantEdge. In this approach, the optimum sets of friction parameters that led to the least deviation from the experimental measurements of orthogonal cutting process were initially determined for each model and the viability of each one was assessed under its optimum condition. Two different working conditions have been considered (K10/AISI 1045 and H13A/AISI 1080) and the following conclusions can be summarized:

- The friction coefficients had a large influence on the FE simulation results. However, the results of the current study indicated that, for both tool-work material combinations and independently of the FE commercial code, nearly an identical range of minimum average error was attained for all adopted friction models.
- The similar range of average error is believed to be due to inability of the JC constitutive model to properly describe the severe deformation condition within the primary and secondary shear zones.
- The analysis of the experimental orthogonal cutting forces indicated the mean Coulomb friction coefficients as high as 1.2 at low ranges of the feed rate.
- The sliding-sticking and pressure-dependent shear friction models provide the most physically relevant expressions for the simulation of frictional condition at the tool-chip interface.

Acknowledgments The authors acknowledge VINNOVA (Swedish Agency for Innovation Systems) within the framework of the FFI programme and the Area of Advance Production at Chalmers University of Technology for financial support. Special thanks are also extended to Adjunct Professor Ibrahim Sadik from Sandvik Coromant for his support.

References

1. Guo YB (2003) An integral method to determine the mechanical behavior of materials in metal cutting. J Mater Process Technol 142: 72–81
2. Bouzakis K-D, Michailidis N, Skordaris G, Bouzakis E, Biermann D, M'Saoubi R (2012) Cutting with coated tools: coating technologies, characterization methods and performance optimization. CIRP Ann Manuf Technol 61:703–723
3. Attanasio A, Ceretti E, Fiorentino A, Cappellini C, Giardini C (2010) Investigation and FEM-based simulation of tool wear in turning operations with uncoated carbide tools. Wear 269:344–350
4. Malakizadi A, Cedergren S, Surreddi KB, Nyborg L (2013) A methodology to evaluate the machinability of Alloy 718 by means of FE simulation. Presented at the Advanced Manufacturing Engineering and Technologies NEWTECH, Stockholm
5. Binder M, Klocke F, Lung D (2015) Tool wear simulation of complex shaped coated cutting tools. Wear 330–331:600–607
6. Özel T (2006) The influence of friction models on finite element simulations of machining. Int J Mach Tools Manuf 46:518–530
7. Kalhori V (2001) Modelling and simulation of mechanical cutting. PhD, Mechanical Engineering, Lulea University of Technology.
8. Rech J, Arrazola PJ, Claudin C, Courbon C, Pusavec F, Kopac J (2013) Characterisation of friction and heat partition coefficients at the tool-work material interface in cutting. CIRP Ann Manuf Technol 62:79–82
9. Svoboda A, Wedberg D, Lindgren LE (2010) Simulation of metal cutting using a physically based plasticity model. Model Simul Mater Sci Eng 18:1–19
10. Chandrasekaran H, M'Saoubi R, Chazal H (2005) Modelling of material flow stress in chip formation process from orthogonal milling and split Hopkinson bar tests. Mach Sci Technol 9:131–145
11. Malakizadi A, Cedergren S, Sadik I, Nyborg L (2016) Inverse identification of flow stress in metal cutting process using Response Surface Methodology. Simul Model Pract Theory 60:40–53
12. Ulutan D and Özel T (2013) Determination of constitutive material model parameters in fe-based machining simulations of Ti-6Al-4V and IN-100 alloys: an inverse methodology. Proc NAMRI/SME. 41.
13. Daoud M, Jomaa W, Chatelain JF, Bouzid A (2015) A machining-based methodology to identify material constitutive law for finite element simulation. Int J Adv Manuf Technol 77:2019–2033
14. Del Prete A, Filice L, Umbrello D (2013) Numerical simulation of machining nickel-based alloys. Procedia CIRP 8:540–545
15. Malakizadi A, Sadik I, Nyborg L (2013) Wear mechanism of CBN inserts during machining of bimetal aluminum-grey cast iron engine block. Procedia CIRP 8:188–193
16. Xu D, Feng P, Li W, Ma Y (2015) An improved material constitutive model for simulation of high-speed cutting of 6061-T6 aluminum alloy with high accuracy. Int J Adv Manuf Technol 79:1043–1053
17. Yang Y, Zhu W (2014) Study on cutting temperature during milling of titanium alloy based on FEM and experiment. Int J Adv Manuf Technol 73:1511–1521
18. Chandrasekaran H, Kapoor DV (1965) Photoelastic analysis of tool-chip interface stresses. J Eng Ind 87:495–502
19. Childs THC (2006) Friction modelling in metal cutting. Wear 260: 310–318
20. Zemzemi F, Rech J, Ben Salem W, Dogui A, Kapsa P (2009) Identification of a friction model at tool/chip/workpiece interfaces in dry machining of AISI4142 treated steels. J Mater Process Technol 209:3978–3990
21. Rech J, Claudin C, D'Eramo E (2009) Identification of a friction model—application to the context of dry cutting of an AISI 1045 annealed steel with a TiN-coated carbide tool. Tribol Int 42:738–744
22. Smolenicki D, Boos J, Kuster F, Roelofs H, Wyen CF (2014) In-process measurement of friction coefficient in orthogonal cutting. CIRP Ann Manuf Technol 63:97–100
23. Merchant ME (1945) Mechanics of the metal cutting process. I. orthogonal cutting and a type 2 chip. J Appl Phys 16:267–275
24. Usui E, Kikuchi K, Hoshi K (1964) The theory of plasticity applied to machining with cut-away tools. J Eng Ind 86:95–104
25. Atkins T (2015) Prediction of sticking and sliding lengths on the rake faces of tools using cutting forces. Int J Mech Sci 91:33–45
26. Zorev NN (1966) Metal cutting mechanics. Pergamon Press, Oxford
27. Hedenqvist P, Olsson M (1991) Sliding wear testing of coated cutting tool materials. Tribol Int 24:143–150
28. Puls H, Klocke F, Lung D (2014) Experimental investigation on friction under metal cutting conditions. Wear 310:63–71
29. Hosseinkhani K, Ng E (2015) A combined empirical and numerical approach for tool wear prediction in machining. Procedia CIRP 31: 304–309
30. Hosseinkhani K, Ng E (2013) Analysis of the cutting mechanics under the influence of worn tool geometry. Procedia CIRP 8:117–122

31. Bil H, Kılıç SE, Tekkaya AE (2004) A comparison of orthogonal cutting data from experiments with three different finite element models. Int J Mach Tools Manuf 44:933–944
32. Arrazola PJ, Villar A, Ugarte D, Marya S (2007) Serrated chip prediction in finite element modeling of the chip formation process. Mach Sci Technol 11:367–390
33. Vaz M Jr, Owen DRJ, Kalhori V, Lundblad M, Lindgren LE (2007) Modelling and simulation of machining processes. Arch Comput Methods Eng 14:173–204
34. Shi B, Attia H (2009) Modeling the thermal and tribological processes at the tool-chip interface in machining. Mach Sci Technol 13: 210–226
35. Puls H, Klocke F, and Veselovac D (2015) FEM-based prediction of heat partition in dry metal cutting of AISI 1045. Int J Adv Manuf Technol. 1–9.
36. Arrazola PJ, Özel TR (2010) Investigations on the effects of friction modeling in finite element simulation of machining. Int J Mech Sci 52:31–42
37. Trent EM, Wright PK (2000) Metal cutting. Butterworth-Heinemann, Boston
38. Iqbal SA, Mativenga PT, Sheikh MA (2007) Characterization of machining of AISI 1045 steel over a wide range of cutting speeds. Part 1: investigation of contact phenomena. Proc Inst Mech Eng B J Eng Manuf 221:909–916
39. Finnie I and S. M. C. (1956) The friction process in metal cutting. *Transactions of ASME 78*. 78:1649–1657.
40. Shirakashi T and U. E. (1973) Friction characteristics on tool face in metal machining. J Japan Soc Precis Eng. 39:966–972.
41. Childs T, Maekawa K, Obikawa T, Yamane Y (2000) Metal machining: theory and applications. John Wiley & Sons Inc., New York
42. Puls H, Klocke F, Lung D (2012) A new experimental methodology to analyse the friction behaviour at the tool-chip interface in metal cutting. Prod Eng 6:349–354
43. Bordin A, Imbrogno S, Rotella G, Bruschi S, Ghiotti A, Umbrello D (2015) Finite element simulation of semi-finishing turning of electron beam melted Ti6Al4V under Dry and cryogenic cooling. Procedia CIRP 31:551–556
44. Jaspers SPFC (1999) Metal cutting mechanics and material behavior. PhD Technische Universiteit Eindhoven.
45. Demuth H and Beale M (1993) Neural network toolbox for use with MATLAB. MathWorks.
46. Marusich TD, Ortiz M (1995) Modelling and simulation of high-speed machining. Int J Numer Methods Eng 38:3675–3694
47. Wang J, Gadala MS (1997) Formulation and survey of ALE method in nonlinear solid mechanics. Finite Elem Anal Des 24:253–269
48. Halim SMT (2008) Finite element modeling of the orthogonal metal cutting process: modeling the effects of coefficient of friction and tool holding structure on cutting forces and chip thickness. PhD, McMaster University.
49. Klocke F (2011) Manufacturing processing I: cutting, RWTH ed.: Springerlink.
50. Guo Z, Saunders N, Schillé JP, Miodownik AP (2009) Material properties for process simulation. Mater Sci Eng A 499:7–13
51. Thepsonthi T, Özel T (2015) 3-D finite element process simulation of micro-end milling Ti-6Al-4V titanium alloy: experimental validations on chip flow and tool wear. J Mater Process Technol 221: 128–145
52. Rotella G, Dillon OW Jr, Umbrello D, Settineri L, Jawahir IS (2013) Finite element modeling of microstructural changes in turning of AA7075-T651 alloy. J Manuf Process 15:87–95
53. Jafarian F, Imaz Ciaran M, Umbrello D, Arrazola PJ, Filice L, Amirabadi H (2014) Finite element simulation of machining Inconel 718 alloy including microstructure changes. Int J Mech Sci 88:110–121
54. Sekhon GS, Chenot JL (1993) Numerical simulation of continuous chip formation during non-steady orthogonal cutting. Eng Comput 10:31–48
55. Iqbal SA, Mativenga PT, Sheikh MA (2007) Characterization of the machining of AISI 1045 steel over a wide range of cutting speeds—part 2: evaluation of flow stress models and interface friction distribution schemes. Proc Inst Mech Eng B J Eng Manuf 221:917–926
56. Klocke F, Raedt HW, Hoppe S (2001) 2D-FEM simulation of the orthogonal high speed cutting process. Mach Sci Technol 5:323–340
57. Ng EG, Aspinwall DK, Brazil D, Monaghan J (1999) Modelling of temperature and forces when orthogonally machining hardened steel. Int J Mach Tools Manuf 39:885–903
58. Bailey JA (1975) Friction in metal machining—mechanical aspects. Wear 31:243–275